

Self-centering Devices with Paralleled Friction Spring Groups: Development, Experiment and System Behavior

Ruixin Zhang, Wei Wang, Cheng Fang, Wenjie Zhang & Lijun Zhuang

To cite this article: Ruixin Zhang, Wei Wang, Cheng Fang, Wenjie Zhang & Lijun Zhuang (2023) Self-centering Devices with Paralleled Friction Spring Groups: Development, Experiment and System Behavior, *Journal of Earthquake Engineering*, 27:3, 520-545, DOI: [10.1080/13632469.2021.2009059](https://doi.org/10.1080/13632469.2021.2009059)

To link to this article: <https://doi.org/10.1080/13632469.2021.2009059>



Published online: 27 Dec 2021.



Submit your article to this journal



Article views: 429



View related articles



View Crossmark data



Citing articles: 10 View citing articles



Self-centering Devices with Paralleled Friction Spring Groups: Development, Experiment and System Behavior

Ruixin Zhang^a, Wei Wang^a, Cheng Fang^a, Wenjie Zhang^b, and Lijun Zhuang^b

^aState Key Laboratory of Disaster Reduction in Civil Engineering & Department of Structural Engineering, Tongji University, Shanghai, China; ^bChina Shanxi Sijian Group Co., Ltd, Taiyuan, China

ABSTRACT

A new self-centering device employing paralleled friction spring groups is developed. The fundamental working principle and fabrication procedure are first presented, followed by quasi-static tests. The devices have flag-shaped hysteretic behavior with excellent self-centering capability and moderate energy dissipation. Stable performance under multiple rounds of loading is also exhibited, suggesting that the devices are fully reusable after undergoing several major earthquakes. A system level analysis is carried out, confirming that the devices are effective in eliminating the residual deformation. A hybrid system is finally proposed enabling a well-balanced control of the peak deformation, residual deformation, and peak floor acceleration.

ARTICLE HISTORY

Received 5 March 2021
Accepted 5 November 2021

KEYWORDS

Friction spring; self-centering; damper; steel braced frame; seismic resilience

1. Introduction

The 2011 Christchurch earthquake caused extensive building damages, and thousands of people were homeless after the earthquake. Many buildings, although not collapsed, were demolished due to excessive damage and residual deformation. It was estimated that the total cost of the reconstruction would be as much as NZD40 billion (GBP20bn), taking up almost 20% of New Zealand's annual GDP (Wood, Noy, and Parker 2016). An independent study (NRC 2011) predicted that in a developed region such as California, a magnitude-7.8 scenario earthquake would have resulted in an estimated USD113 billion in damages to buildings and lifelines, and nearly USD70 billion in business interruption. The impact of a major earthquake is often long lasting, mainly because of the lengthy process of recovery. The permanent structural and non-structural damages are difficult and time-consuming to repair, and the cost of repair could exceed that of rebuilding a new structure when the residual deformation exceeds a certain threshold, e.g., 0.5% inter-story drift (McCormick et al. 2008).

Seismic resilient design, a step forward from the conventional seismic-resistant design, aims to significantly reduce the disruptions to life and economy in the aftermath of strong earthquakes (Jiang et al. 2019a, 2019b). "Self-centering capability" is recognized as one of the most important characteristics that promote structural resiliency. An early attempt was to use post-tension (PT) tendons in steel beam-to-column connections, where recoverable rotation is provided by the PT tendons when gap opening occurs at the contacting interface between the beam end and the column, with energy dissipation offered by steel angles or friction pads (Li, He, and Wang 2018; Lin, Sause, and Ricles 2013; Ricles et al. 2001, 2002; Zhang et al. 2016). While such systems were found to exhibit reliable flag-shaped hysteretic behavior with no residual deformation, some practical issues were later identified which may hinder the application. For example, the on-site installation of the PT tendons is technically demanding and induces undesirable large initial



compression to the steel beams. In addition, the gap opening mechanism can result in a detrimental “beam-growth effect” when the rigid end of the beam tries to rotate about the turning point on the column surface. This effect results in an increase in the distance between the beam points of inflection and could cause damage to the floor diaphragm. Improvements have been made by revising the details of either the connections (Fang, Wang, and Feng 2019; Feng, Fang, and Wang 2019; Khoo et al. 2013, 2012) or the flooring system (Chou and Chen 2011a, 2011b; Garlock and Li 2008).

In addition to the extensive investigations on self-centering connections, self-centering braces emerged as a promising alternative which seems to gain increasing popularity because they are easier to install (field tensioning is not necessary), induces no beam-growth, and can be potentially commercialized. Utilizing the PT-based technique, Christopoulos et al. and Erochko et al. (Christopoulos et al. 2008; Erochko, Christopoulos, and Tremblay 2015a; Erochko et al. 2013) successfully developed a series of pioneering self-centering braces capable of providing recoverable deformation and large load carrying capacity. However, the maximum deformability of such braces is largely restricted by the small available elastic strain of the PT tendons, a case which limits the maximum peak inter-story drift that the braces can provide. Realizing this critical issue, Erochko et al. (Erochko, Christopoulos, and Tremblay 2015b) and Chou et al. (Chou et al. 2014, 2016) proposed dual-core self-centering braces with increased brace deformability. Nevertheless, existing studies (Fang et al. 2018, 2021; Ping et al. 2021; Qiu and Zhu 2016) suggested that the deformation demand of a self-centering frame under strong or pulse-like near-fault earthquakes could still well exceed the ductility supply of the improved PT-based braces.

In order to ensure reliable performance of self-centering braces at large deformation, the potential of new materials or new elements have been recently explored. The former solution mainly focused on shape memory alloys (SMAs) (Fang et al. 2014, 2017, 2016, 2015a; Qiu et al. 2017; Yam et al. 2015; Wang, Fang, and Liu 2017; Wang et al. 2017, 2019a; Miller, Fahnstock, and Eatherton 2012; Qiu and Zhu 2017a, 2017b) and fiber-reinforced polymer composites (Xie et al. 2017; Zhou et al. 2015). In particular, the superelasticity exhibited by the SMAs enables a spontaneously recoverable strain of 8 ~ 10%, accompanied by inherent energy dissipation under cyclic loading (Fang et al. 2015b; Wang, Fang, and Liu 2016; Xu, Zhang, and Luo 2016). Alternatively, the tendons can be replaced by compression springs which serve a similar purpose but could be more adaptable in providing load resistance and deformability. Xu et al. (Xu, Fan, and Li 2016, 2017a, 2017b) experimentally verified a new type of self-centering damper with disc springs (washer springs). Dong et al. (Dong et al. 2017) upgraded the conventional buckling restrained braces (BRBs) by introducing an extra set of disc springs to encourage self-centering capability. Fang, Wang, and Shen (2021) and Wang et al. (2021) recently proposed new disc spring-based self-centering braces for seismic hazard mitigation. Apart from disc springs, friction springs have also been considered as kernel elements for self-centering devices, noting that such springs have the largest load carrying capacity among all the available spring types (Bruneau and MacRae 2017; Filiatru, Tremblay, and Kar 2000; Hill 1995; Riley et al. 2006). More recently, the authors and co-workers proposed a new self-centering device incorporating a single set of friction springs (Wang et al. 2019b), where the feasibility was experimentally verified. The practical use of friction springs was also promoted during the reconstruction of Christchurch after the earthquake in 2011.

Following the previous work, this study sheds further light on the application of friction springs for self-centering devices suited to braced frames. In particular, paralleled friction spring groups are proposed to reduce the necessary size of the device. The potential advantages of the proposed device include large initial stiffness, adaptable deformability, adjustable load carrying capacity, excellent self-centering capability and reliable energy dissipation. This study commences with a detailed description of the working mechanism, analytical expression and fabrication process of the device, followed by physical tests on three small scale device specimens varied in the taper surface treatments of the friction springs (to achieve different frictions). In addition, multiple rounds of tests were conducted on each device specimen to examine their performance under sequential earthquakes, e.g., mainshock-

aftershock sequences. With confidence gained from the experimental results, a prototype building is designed and a system-level analysis is performed to understand the dynamic behavior of the braced frames incorporating the proposed self-centering devices.

2. Working Mechanism

2.1. Introduction to Friction Springs

Friction springs are mechanical components used in the civil and military-related industries. A friction spring group consists of a series of outer and inner rings assembled alternately with tapered mating surfaces, as shown in Fig. 1a. When subjected to compression, friction springs can develop very large load resistance with considerable energy dissipation provided by the friction between the outer and

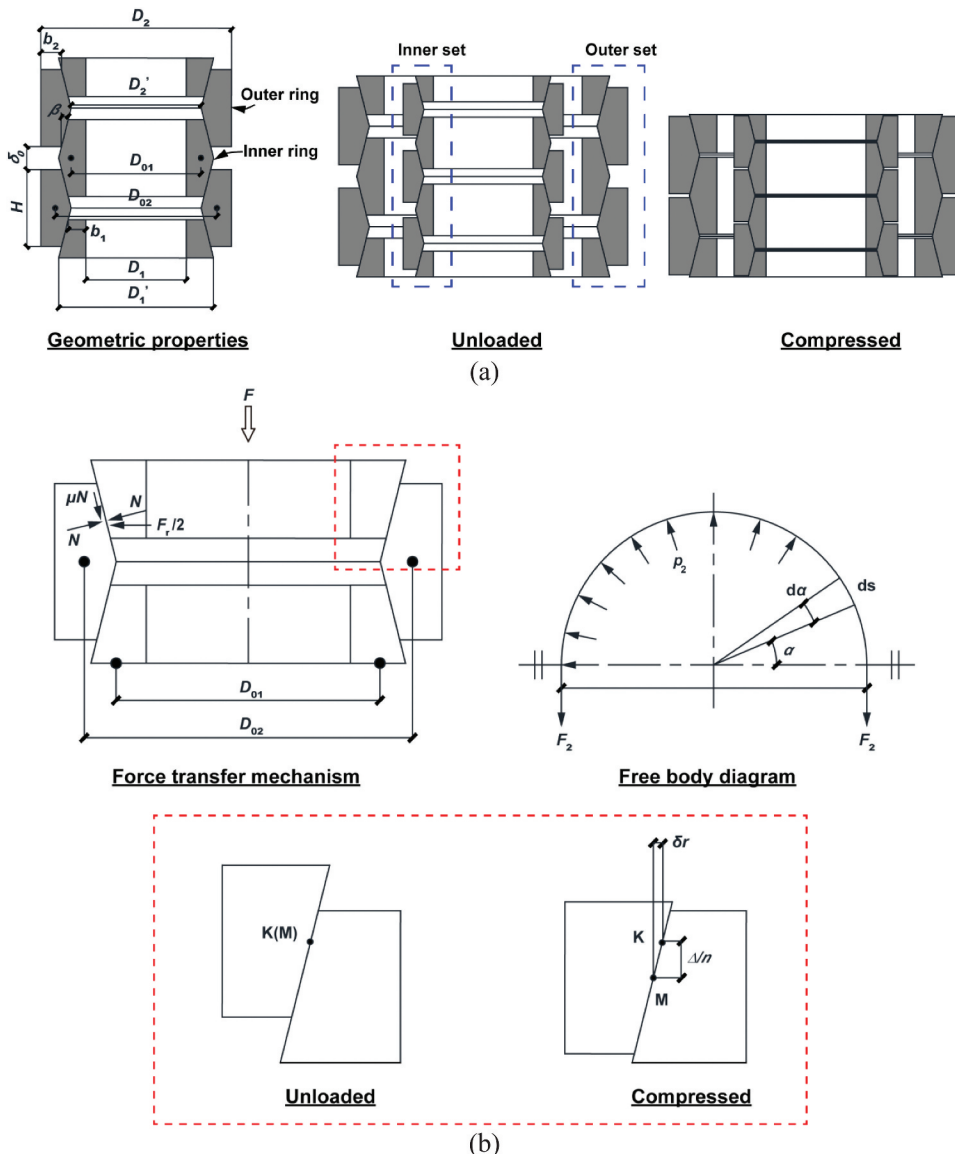


Figure 1. Friction springs: a) geometric properties, b) force transfer mechanism.

inner rings. The overall deformability of a friction spring group can be simply adjusted by changing the number of rings placed in series, although the maximum number of rings is limited by the allowable length of the device. While the load carrying capacity is not directly dependent on the number of the rings, paralleled ring spring groups, as illustrated in Fig. 1a, can be adopted to increase the total load resistance.

Figure 1b further illustrates the force transfer mechanism of the friction springs. The hoop stress in the outer ring (σ_2) and the inner ring (σ_1) can be estimated by:

$$\sigma_2 = \frac{F}{\pi A_2} \left(\frac{\cos \beta - \mu \sin \beta}{\sin \beta + \mu \cos \beta} \right) = \frac{F}{\pi A_2 \gamma}, \text{ and } \gamma = \tan(\beta + \rho) \quad (1)$$

$$\sigma_1 = \frac{F}{\pi A_1} \left(\frac{\cos \beta - \mu \sin \beta}{\sin \beta + \mu \cos \beta} \right) = \frac{F}{\pi A_1 \gamma} \quad (2)$$

where F is the overall load resistance of the system, A_1 and A_2 is the cross-section area of the inner ring and the outer ring, respectively, β is the taper angle, as shown in Fig. 1a, and μ ($\mu = \tan \rho$) is the friction coefficient over the taper surface.

The total compressive deformation (Δ) can be derived based on the following geometric relationship:

$$\Delta = \frac{n \cdot \delta r}{\tan \beta} = \frac{\sigma_1 D_{01} + \sigma_2 D_{02}}{2E \tan \beta} \quad (3)$$

where n is the total number of the contacting pairs in a friction spring group, E is the Young's modulus, D_{01} and D_{02} is the equivalent diameter of the inner ring and the outer ring measured according to the centroid of the cross-section, respectively, as shown in Fig. 1a, and δr is the sum of the radial deformation contributed by both the outer and inner rings, as illustrated in Fig. 1b. As shown in Fig. 2a, a friction spring group responds to the applied compression (F) with a linear load-deformation response. The ascending stiffness ($K = F/\Delta$) can be expressed by:

$$K = \frac{2\pi E y \tan \beta}{n \left(\frac{D_{01}}{A_1} + \frac{D_{02}}{A_2} \right)} \quad (4)$$

Considering a reversed friction action, the unloading stiffness (K') can be expressed by:

$$K' = \frac{2\pi E y' \tan \beta}{n \left(\frac{D_{01}}{A_1} + \frac{D_{02}}{A_2} \right)}, \text{ and } y' = \tan(\beta - \rho) \quad (5)$$

The area enveloped by the triangle is essentially the energy dissipation during that loading cycle. The behavior of friction springs used for the proposed device was investigated via a preliminary experimental study, where Fig. 2a compares the test results with the analytical predictions, where satisfactory agreements are observed. As shown in Fig. 2b, the tests were conducted quasi-statically under displacement control through a universal test machine (UTM). The test setup included a loading plate and a base plate which were fixed to the top and bottom wedge hydraulic grips, respectively. The individual friction spring specimens were made of 60Si2MnA (typical spring steel) with a nominal minimum yield strength of 1375 MPa, and they were shot blasted for 15 minutes followed by phosphorization. The purpose of phosphorization is to improve the wear properties and corrosion resistance of the friction springs. Apart from the light grease in the as-received condition, no further grease was applied between the outer and inner rings. For the analytical predictions, a friction coefficient of $\mu = 0.1$ was assumed as suggested by the supplier. While the use of $\mu = 0.1$ leads to good agreements, the precise friction coefficient is in fact difficult to measure, so using a guessed value of μ which fits the test result may be the most convenient way. It should be noted that increasing the

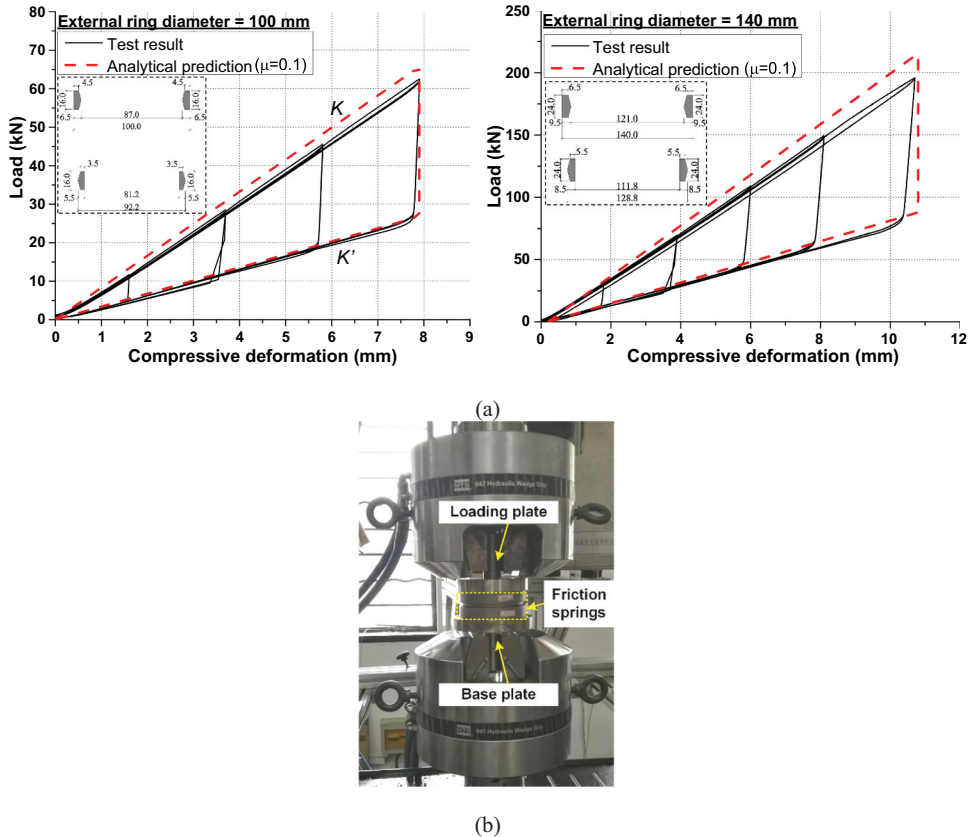


Figure 2. Behavior of friction springs: a) comparison between analytical prediction and test result, b) test setup.

friction could decrease the recoverability of the friction springs, so an overly large friction is not recommended. It is also noted that the two friction spring sets may not be exactly the same length at the start even though they are designed as the same length (due to the machining tolerance of the friction ring springs). However, this is not a big issue because the two ring spring sets would share load according to their loading stiffness as expected after precompression. According to the ascending stiffness (K), when the precompression deformation (Δ_{pre}) is determined, the precompression force (i.e., "yield" strength of the device, F_y) can be estimated by:

$$F_y = K \cdot \Delta_{pre} \quad (6)$$

The recommended precompression process is discussed later in Section 2.3.

2.2. Working Mechanism of Device

The device proposed in the present study is designed such that the friction spring groups are always subjected to compression regardless of the loading status of the device itself. This working mechanism is realized by a specially detailed piston type device, and the deformation mode of the device is illustrated in Fig. 3. The device consists of an external tube, an internal shaft, precompressed friction spring groups in between, and other necessary accessories including hinged ear plates, shim plates, tightening nuts and a guide tube. To facilitate fabrication, the external tube has to be separated into two parts which are later assembled through the threaded junction. In order to satisfy the load resistance demand, it is likely that the diameter of the device is larger than the width of the column

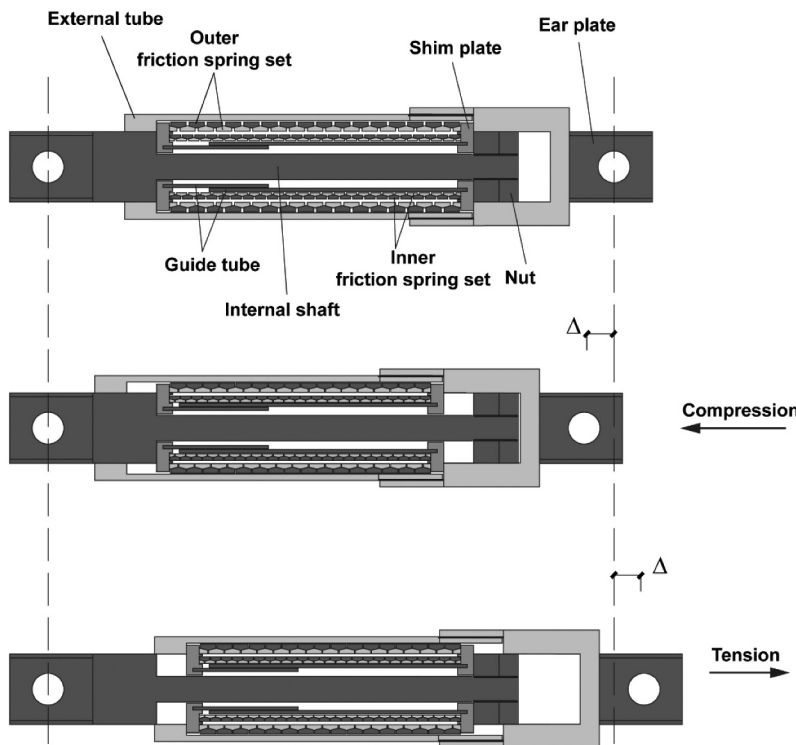


Figure 3. Working principle of proposed device.

when a single set of friction springs are used, making the installation of the device difficult, and also affecting the aesthetics of the building. Hence, self-centering devices with paralleled friction spring groups are proposed to reduce the size (diameter) of the device with the same load carrying capacity maintained, or to effectively improve the load resistance of the device with the same size. The current figure shows a typical case where two sets of friction springs are placed in parallel (hereafter called “outer friction spring set” and “inner friction spring set”). For typical sizes of commercial friction springs, the force capacity can be increased by about 40% to 80% compared with only using the outer set of friction springs.

One challenge of employing paralleled friction spring groups is the effectiveness of the guides, because a “long” friction spring group tends to lose stability under compression (a phenomenon which is similar to the global buckling of slender compression members). Guides which prevent excessive transverse movement of the friction springs are necessary. For the proposed damper configuration, the external tube serves as the guide for the outer friction spring set, and an additional guide tube is used for the inner set. For both sets, a small radial clearance should be left to allow free expansion/contraction of the rings. Although not attempted in the present study, more sets of friction springs can be used to further increase the load resistance of the device, as long as appropriate guides are provided, but this clearly complicates the design and manufacturing of the device.

2.3. Recommended Fabrication Process

Figure 4 gives a detailed demonstration of the recommended fabrication steps for a typical device employing two sets of friction spring groups placed in parallel. A work station and a temporary base block are first prepared (step 1), and the lower shim plate is placed in position above the base block. The guide tube is placed and the friction springs are then installed one by one, during which process

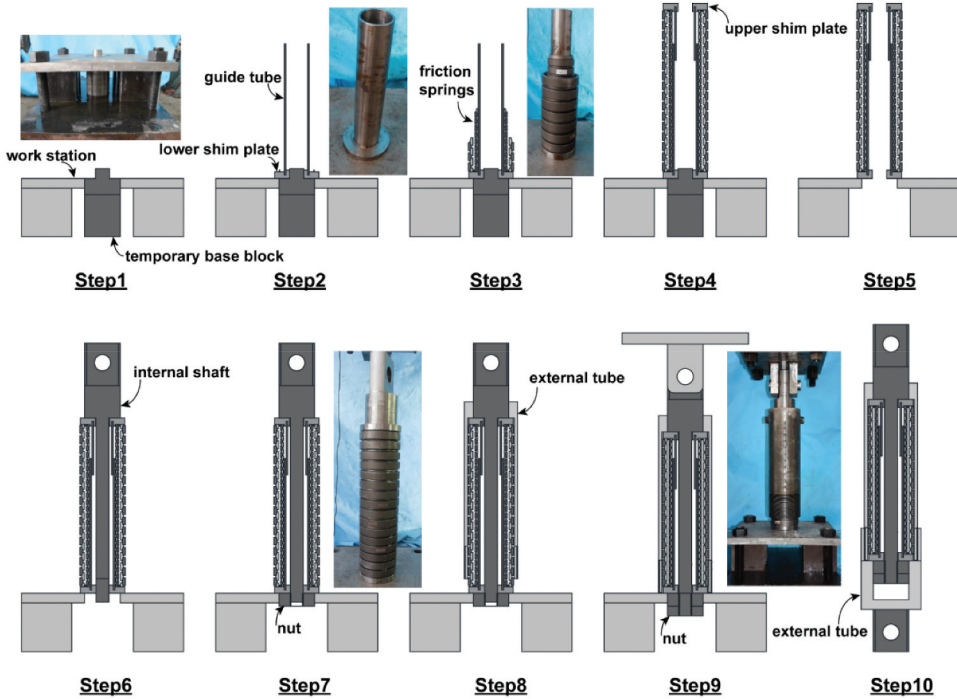


Figure 4. Fabrication process of proposed device.

a level ruler could be used to ensure that the rings are properly placed with no obvious tilt (steps 2–3). Once the installation of the friction springs and the upper shim plate is finished, the temporary base block can be removed (step 4–5). The internal shaft then passes through the friction springs (step 6), and the tightening nut can be manually screwed using the available space previously occupied by the base block (step 7). Part of the external tube is then installed (step 8) and the friction springs are now ready for precompression. It is noted that the “yield” resistance of the device is directly related to the precompression level of the friction springs, and moreover, the precompression ensures that a reasonably large initial stiffness is maintained before decompression. A large precompression is often required, so is the necessary torque applied to the tightening nuts. This makes manual operation infeasible, so a hydraulic actuator is recommended for applying the precompression. As illustrated in step 9, the load can be gradually applied from the top connector, and the nuts at the bottom are further tightened by a wrench in the meantime. Double nuts could be employed to reduce loss of precompression. The fabrication process ends with the installation of the remaining part of the external tube (step 10).

3. Experimental Study

3.1. Test Specimens

Three small scale prototype device specimens were produced and tested quasi-statically. The specimens have the same geometric details, as shown in Fig. 5. Each device included two sets of friction spring groups. The largest diameters of the outer rings used for the outer and inner friction spring sets are 140 mm and 100 mm, respectively, and more details of the rings are given in Table 1, where H , D_1 , D_2 , β , b_1 and b_2 are geometric parameters of the inner and outer rings, as marked in Fig. 1a. The precompression was consistently taken as 40 mm, corresponding to a target load resistance of approximately 100 kN and 40 kN for the outer and inner sets (assuming $\mu = 0.1$), respectively. The external tube and internal

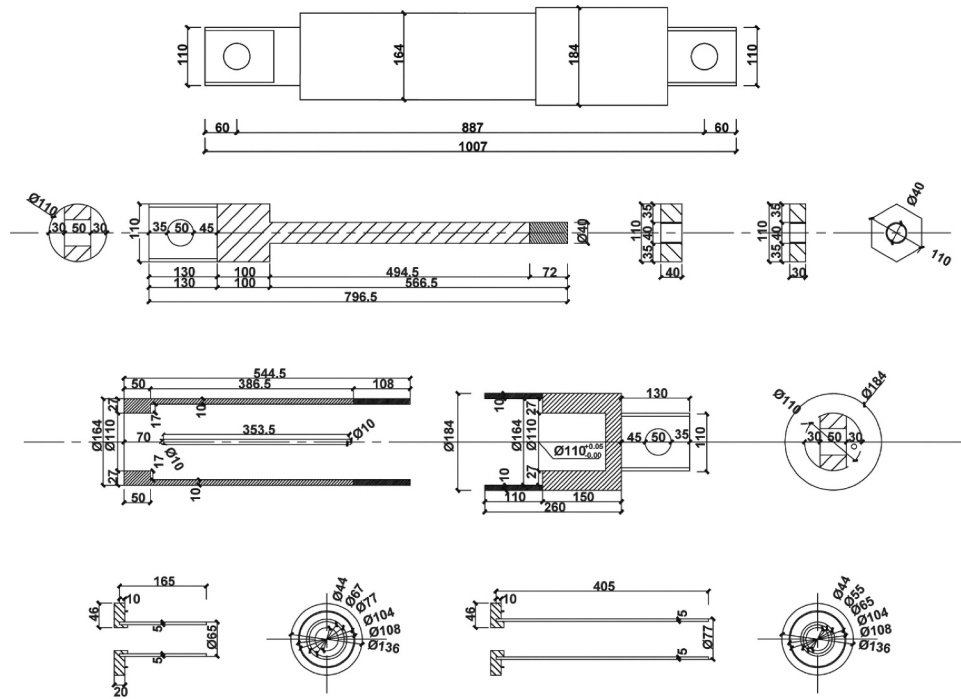


Figure 5. Key dimensions of device specimen.

Table 1. Key dimensions of individual friction springs.

Location	Ring type	H (mm)	D_2 or D_1 (mm)	$\beta\beta$	b_2 or b_1 (mm)
Outer set	Outer rings	24	140	14.03°	6.5
	Inner rings	24	111.8	14.03°	5.5
Inner set	Outer rings	16	100	14.03°	4.5
	Inner rings	16	81.2	14.03°	3.5

shaft were made of Q235 steel (nominal yield stress $f_y = 235$ MPa) and 38CrMoAl alloy, respectively, and the material for the friction springs was the same as that discussed in Section 2.1. The fabrication process for the specimens was consistent with that presented in Fig. 4. A hydraulic actuator was used for applying the precompression. The entire precompression procedure was controlled by measuring the vertical movement of the actuator.

For each device, the outer friction spring set consisted of 16 outer rings and 17 inner rings (including half inner rings), and the inner set consisted of 24 outer rings and 25 inner rings. The nominal maximum deformability of the considered friction spring groups at a fully-compressed status was 115.2 mm, and by deducting the precompression of 40 mm, the available deformability was actually 75.2 mm. The three specimens varied in the treatment of the friction interfaces between the outer and inner rings. Three different surface treatments for the friction springs were considered, namely, no shot blasting (specimen NS), shot blasting for 15 minutes (specimen S15), and extended shot blasting for 25 minutes (specimen S25). Given that lubricant could also be an influential factor, grease was particularly applied for the friction springs used for specimen NS to reduce the friction over the taper surface, whereas no grease was applied for the other two specimens.

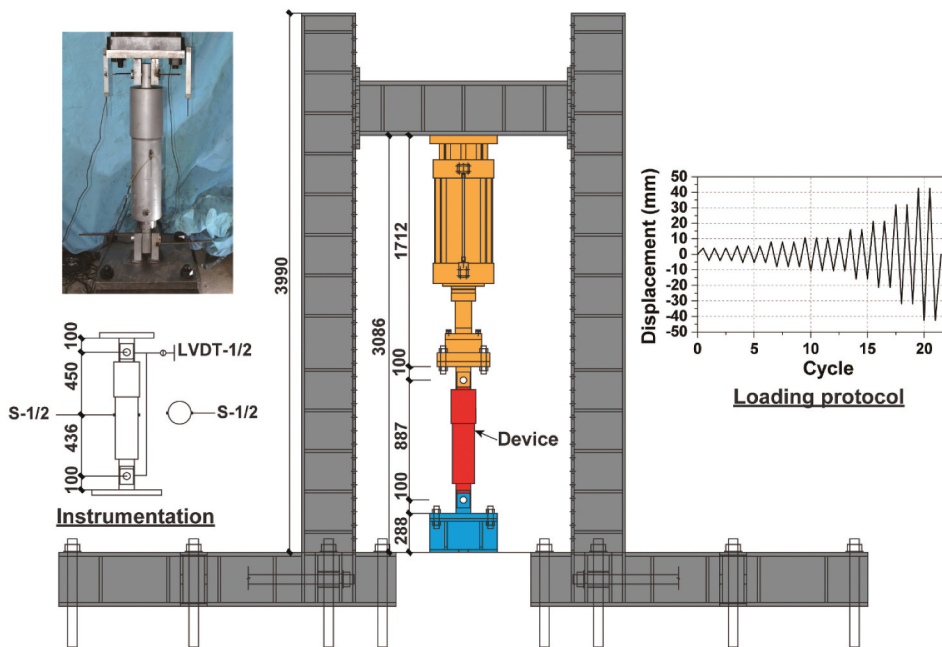


Figure 6. Test setup and instrumentation for device specimens.

3.2. Test Arrangement

Isolated devices were tested in the current study. The test setup was designed such that the axial behavior of the devices is adequately captured, as shown in Fig. 6. The specimen was vertically placed and the ear plates at the two ends were connected to the test rig. The cyclic load was quasi-statically applied through a servo-controlled hydraulic actuator. The instrumentation is also illustrated in Fig. 6. Two vertical LVDTs (linear variable differential transformers) were used to record the axial deformation of the specimens, and a pair of strain gauges were placed on the surface of the external tube to make sure that the load was applied concentrically, and also to check if the component stayed elastic throughout the testing process. The condition of the friction springs could be visually monitored through the observation slits opened on the external tube. The loading protocol is shown in Fig. 6 (Clark et al. 1997), where the maximum considered deformation was 42.5 mm. The entire step-wise loading process shown in the figure was repeated for three times (round 1 to round 3) to examine the reliability of the device under sequential earthquakes, and to confirm if the devices are reusable.

3.3. General Test Observations

The three device specimens showed anticipated deformation mode. It was clearly seen from the observation slits that the friction springs were compressed when the specimens were loaded. The typical conditions of the specimens at varying stages are shown in Fig. 7a, and the same behavior was observed during the three repeated rounds of testing. It is believed that the main deformation was indeed provided by the friction springs while the other components behaved elastically. For instance, the strain gauge readings (for the external tube), as typically shown in Fig. 7b, indicate that the maximum microstrain (ε_μ) is approximately 260, which is much smaller than the nominal yield strain of Q235 steel ($\varepsilon_\mu = 1150$). It is also found that the strain of the external tube is close to zero when the device is in compression but increases when the device is in tension. This is explainable by checking the proposed working mechanism of the device, as previously illustrated in Fig. 3.

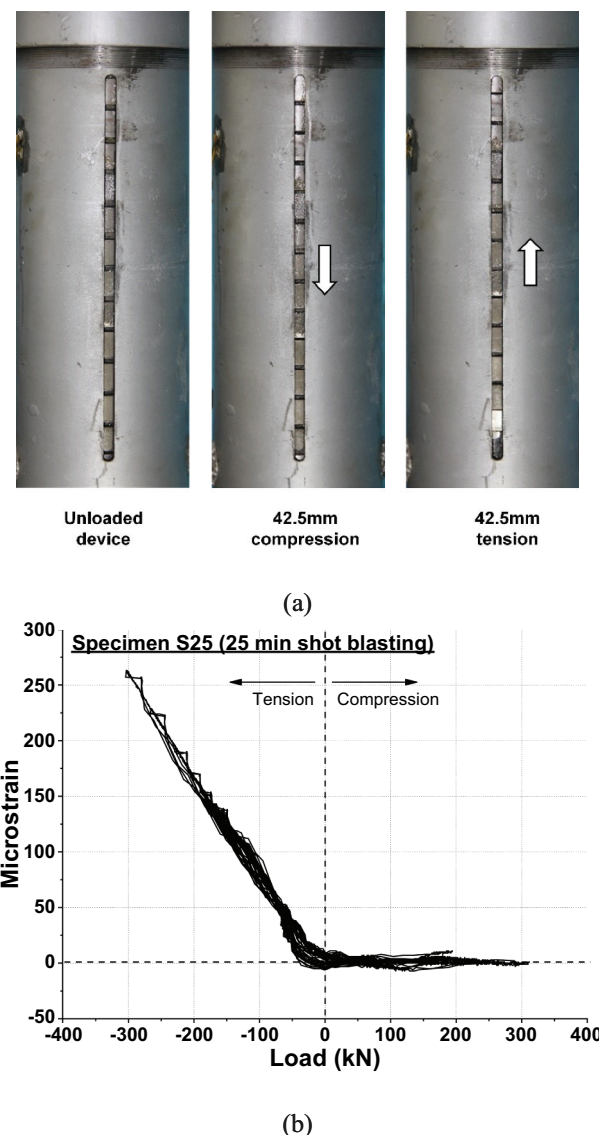


Figure 7. Test observations: a) deformation behavior, b) typical strain gauge reading.

Another observation was that the friction springs were unevenly compressed (i.e., the widths of the gaps were not identical), especially at large deformations. This is not an uncommon phenomenon because the rings may experience minor inclination when the friction spring group has a “global buckling” tendency. As appropriate guides are provided for the friction springs and hence excessive transverse deflections are prohibited, the inconsistent deformation and slight inclination of individual rings should have little detrimental effect on the overall behavior of the device. It is also noticed that the friction springs were not fully compressed at 42.5 mm. As mentioned previously, the remaining deformability serves as a margin for unexpected deformation demand under rare earthquakes beyond the maximum considered earthquake (MCE). After finishing the necessary rounds of testing, the specimens were disassembled. Detailed inspections showed that apart from minor abrasion over the friction interface between the inner and outer

rings, all the components and junctions (e.g., the threaded junction between the two parts of the external tube) were intact, implying reliable performance of the proposed device after experiencing multiple major earthquakes.

The stable behavior of the device can be better revealed by the load-deformation hysteretic curves, as shown in Fig. 8. Typical flag-shaped responses are observed, and importantly, almost no degradation is exhibited under the three repeated rounds of loading. This indicates that the friction springs are durable elements, and stable frictional forces are provided. Moreover, the initial stiffness of the device is quite large, which is an important characteristic because the bracing systems incorporating these devices are supposed to resist lateral load (such as wind) with strictly controlled deformation. The “yield” strength is consistent with the preload applied to the friction springs, followed by a plateau with the post-yield stiffness which is expressed by Eq. (10). Upon unloading, the reversed friction causes an abrupt drop of the resisting load, and then a reversed plateau with the stiffness given by Eq. (11) is exhibited. The different treatments of the taper surface is shown to affect the overall hysteretic behavior. In general, the shot blasting process increases the friction and hence widens the hysteresis. However, further increasing the shot blasting time from 15 min to 25 min seems to be less influential.

3.4. Discussion of Test Results

Table 2 summarizes in more detail the strength, stiffness, self-centering capability and energy dissipation characteristics of the three device specimens. The “yield” load (F_y) ranges from 118.5 to 148.7 kN and increases with increasing frictional force of the taper surface. A similar trend is observed for the maximum load (F_{max}) at 42.5 mm deformation. Both F_y and F_{max} show little sensitivity to the repeated rounds of cyclic loading. According to the theoretical calculation, around 70% of the load resistance is contributed by the outer friction spring set, and the remaining 30% is contributed by the inner set. In other words, compared with the case of using only one set of friction springs (e.g., the outer set only), the paralleled arrangement increases the load resistance by 40% without increasing the necessary size of the device. The over-strength ratio, i.e., F_{max}/F_y ratio, of the current specimens is 2.2 on average. The notable over-strength is on one hand, beneficial for avoiding soft story mechanism especially when the P-Δ effect is pronounced at large inter-story drifts (Gupta and Krawinkler 1998), but on the other hand, tends to impose larger load to the adjacent members and hence should be carefully considered when designing the boundary frames and brace-to-frame connections.

For the stiffness response, the initial stiffness (K_i) given in Table 2 was measured by establishing a secant line passing from the origin to the yield point, based on the skeleton curve of the hysteretic response. The value of K_i ranges from approximately 210 kN/mm to 245 kN/mm, varying with the different specimens and showing minor sensitivity to the different rounds of loading. In fact, the initial stiffness response of the proposed self-centering devices is related to many factors such as the level of prestressing, level of tightening (when installing of the second part of the external tube), elastic deformation of the other device components, and possible machining tolerance (e.g., uneven bearing surface). Huang et al. (Huang, Eatherton, and Zhou 2020) concluded that the actual initial stiffness of PT-based self-centering systems is difficult to predict using theoretical equations due to the uncertainties related to manufacturing and fabrication. In general, the “secant line approach” used in this study is on the conservative side, i.e., lower bound initial stiffness is given. As shown in Fig. 9, if the specimen was tested only within its “elastic range”, the elastic stiffness is typically larger than those obtained from the secant line approach. Table 2 also gives the post-yield stiffness (K_p) which is essentially the ascending stiffness of the friction spring groups after decompression, i.e., Eq. (10). The K_p/K_i ratio ranges between 1.4% and 1.8%, which is similar to or slightly smaller than that of metallic dampers (including BRBs) where the K_p/K_i ratio is typically 2 ~ 5%.

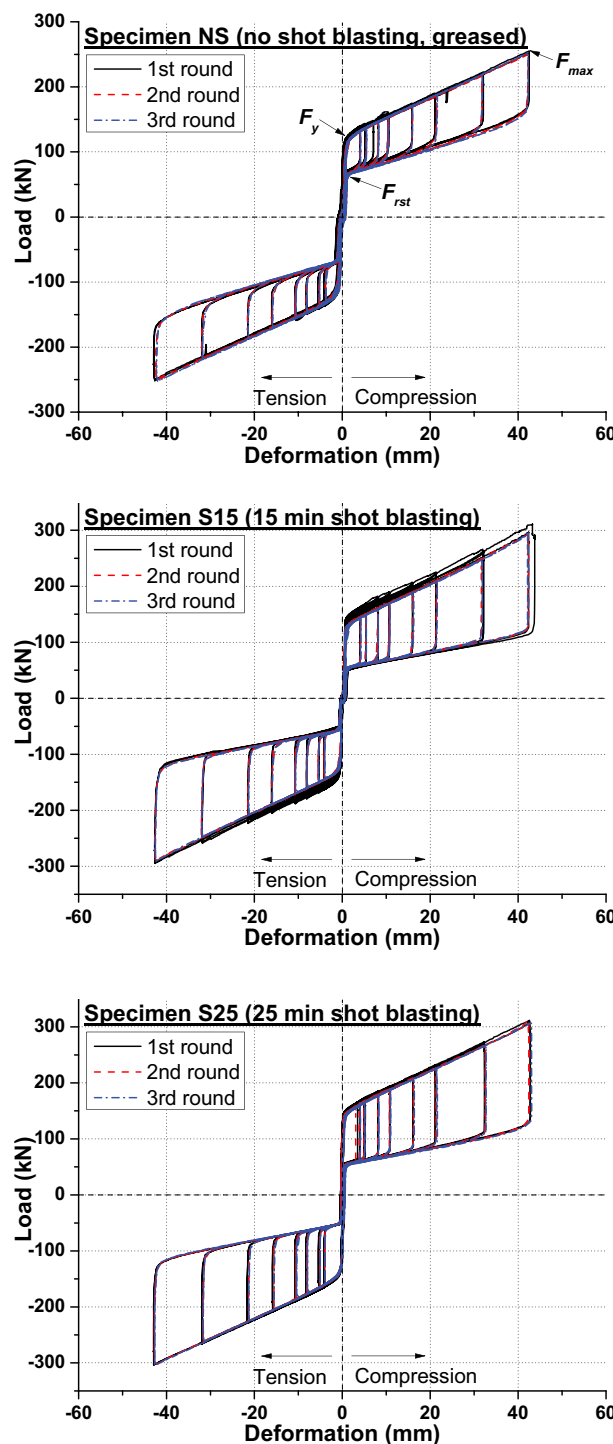


Figure 8. Load-deformation hysteretic responses of device specimens.

Table 2. Summary of device test results.

Specimen	Test round	Yield load F_y (kN)		Maximum load* F_{max} (kN)		Initial stiffness K_y (kN/mm)		Post-limit stiffness K_p (kN/mm)		Restoring force F_{rst} (kN)	
		Measured	Predicted	Measured	Predicted	Measured	Predicted	Measured	Predicted	Measured	Predicted
NS	1 st	119.9	120.7	254.4	249.0	214.44	3.14	3.02	70.6	78.5	6.1
	2 nd	118.5	249.3	252	210.93	3.16	68.1				6.3
	3 rd	118.9				3.20	67.1				6.5
S15	1 st	142.1	142.6	308.9	294.2	208.14	3.84	3.57	51.3	58.1	9.7
	2 nd	130.2		292.5		210.53	3.62		54.9		10.6
	3 rd	128.6		293		225.91	3.70		55.2		13.5
S25	1 st	148.7	151.6	310.8	312.6	244.18	3.76	3.79	52.7	50.1	13.1
	2 nd	145.7	144.7	310		231.88	3.77		53.3		10.2
	3 rd			311.3		238.28	3.81		52.5		12
											14.5
											14.7
											12.1
											14.7

Note: * representative values at the ± 42.5 mm cycle

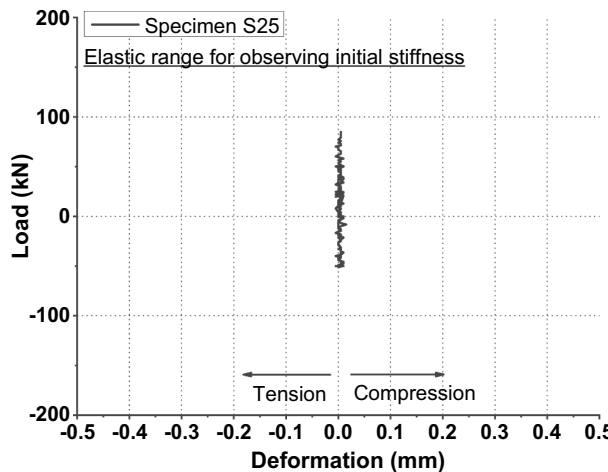


Figure 9. Initial stiffness of specimen tested within its elastic range.

The self-centering capability can be quantitatively evaluated by the restoring force F_{rst} , as marked in Fig. 8. A larger F_{rst} leads to increased self-centering tendency but decreased energy dissipation. Taking specimen S15 for instance, the value of F_{rst} is around 53 kN, corresponding to a F_{rst}/F_y ratio of 0.39. Existing system level analysis indicated that an overly large F_{rst}/F_y ratio is detrimental to inter-story drift and floor acceleration control (Fang et al. 2018). It is also found that an F_{rst}/F_y ratio being larger than 0.5 could lead to undesirable high mode effect (Qiu and Zhu 2016). These phenomena will be reaffirmed through the system-level analysis presented later in Section 4. Therefore, a balance between self-centering capability and energy dissipation should be maintained, and from the perspective of peak response control, a reasonably small restoring force is preferable.

The absolute energy dissipation per cycle (W_D) and the equivalent viscous damping (EVD) as a function of cycle number are shown in Fig. 10a and b, respectively. Note that W_D is essentially the area of the hysteresis during each cycle, and EVD is a dimension-independent index given by:

$$EVD = \frac{W_D}{4\pi W_E} \quad (7)$$

where W_E is the strain energy in a linear system. Typical values of W_D and EVD at the deformation of 42.5 mm are also summarized in Table 2. As expected, increasing the friction of the taper surface enhances the energy dissipation capacity. For instance, specimen S25 has energy dissipation per cycle about two times that of specimen NS in the last cycle. Although not directly obtained from the test, it is estimated from the theoretical expression that the outer friction spring set contributes to approximately 70% of the total energy dissipation, and the remaining 30% is contributed by the inner set. The EVD ranges from 10% to 20%, where the value decreases with increasing amplitudes due to the fact that the strain energy increases at a higher rate compared to the dissipated energy.

3.5. Analytical Predictions

By properly considering the precompression of the friction springs, the analytical model presented in Section 2.1 can be employed to construct the entire hysteretic curves of the device specimens. With the initial precompression deformation (Δ_{pre}) and other geometric details known, and assuming an appropriate friction coefficient (μ), the predicted post-yield stiffness (K), the unloading stiffness (K') and the yield load (F_y) of the device can be easily derived from Equations. (4) to

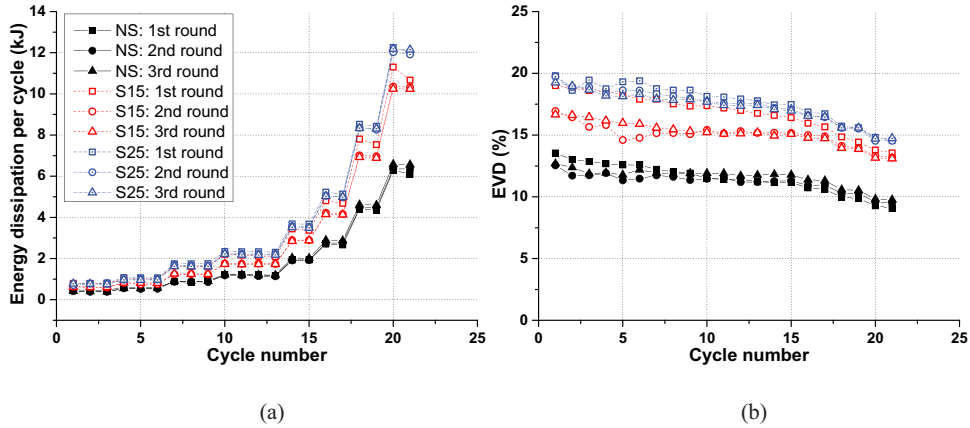


Figure 10. Energy dissipation characteristics of device specimens: a) energy dissipation per cycle, b) EVD.

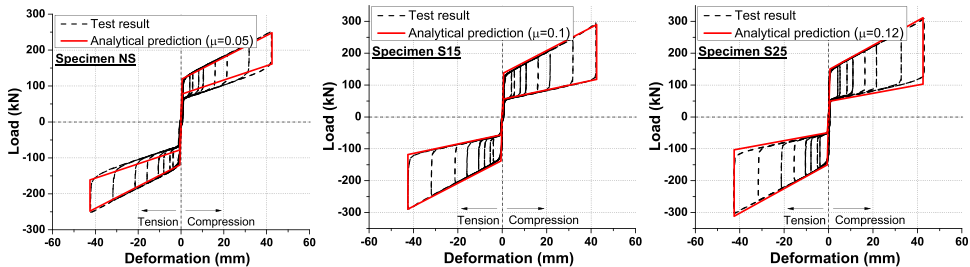


Figure 11. Comparison between test results and analytical predictions.

(6), as listed in **Table 2**. The analytical predictions agree quite well with the test results as shown in **Fig. 11**. The minor discrepancy may be attributed to the uncertainty related to the friction coefficient and possible machining tolerance of the friction springs and other components. One big challenge is the difficulty in arriving to a definitive design prediction of the initial stiffness, and therefore the measured values given in **Table 2** are temporarily used in the analytical prediction. In practice, empirical values based on the existing testing data pool can be used, or field testing is conducted to directly obtain the actual initial stiffness.

4. System-level Analysis

4.1. Prototype Buildings

A system-level analysis is conducted to further demonstrate the effectiveness of the proposed device in seismic control. To facilitate comparison, three six-story prototype steel braced frames are considered, namely, self-centering braced frame (SC-BF), buckling-restrained braced frame (BRBF), and hybrid braced frame (HBF). The geometric configuration of the three frames, which only differ in the brace design, is illustrated in **Fig. 12**. The three buildings are assumed to locate at a Class C site in Seattle, Washington, and the following design response spectral values are assigned: $S_{DS} = 1.09$ g, $S_{D1} = 0.494$ g, and $T_L = 6$ s, where S_{DS} and S_{D1} are the design spectral response acceleration parameters at short periods and 1 s, respectively, and T_L is the long-period transition period (ASCE 7-16 2016)). **Figure 13** shows the 5% damped individual and mean elastic response spectra of the 20 design based earthquake (DBE, i.e., probability of exceedance of 10% in 50 years) ground motions developed for the

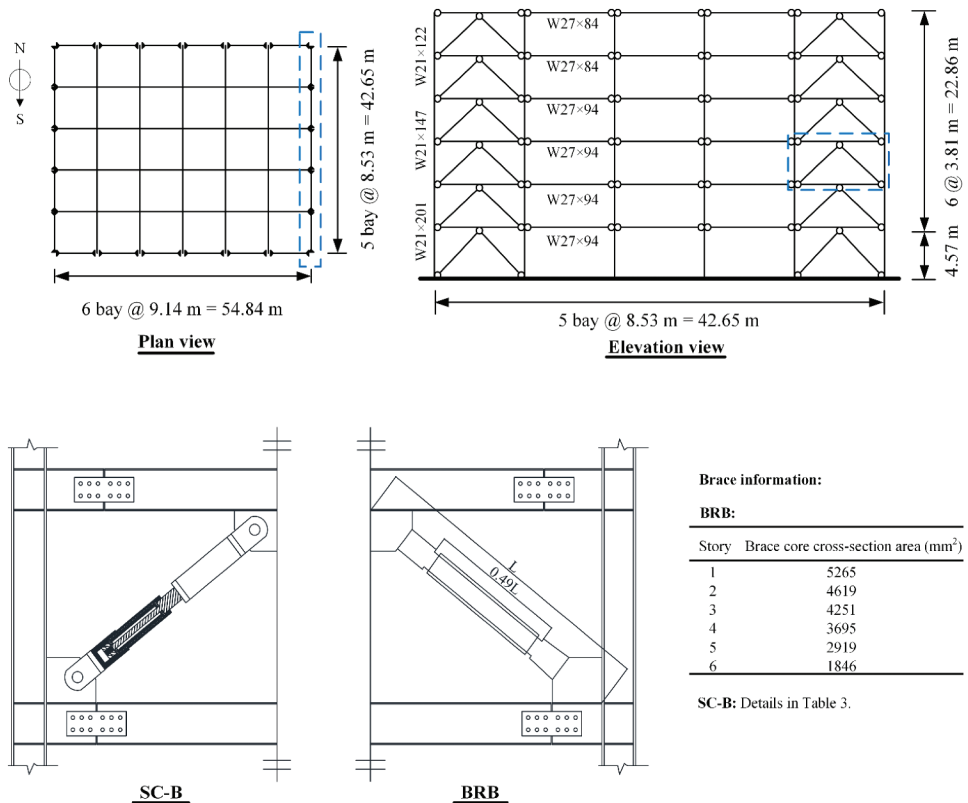


Figure 12. Information of prototype buildings.

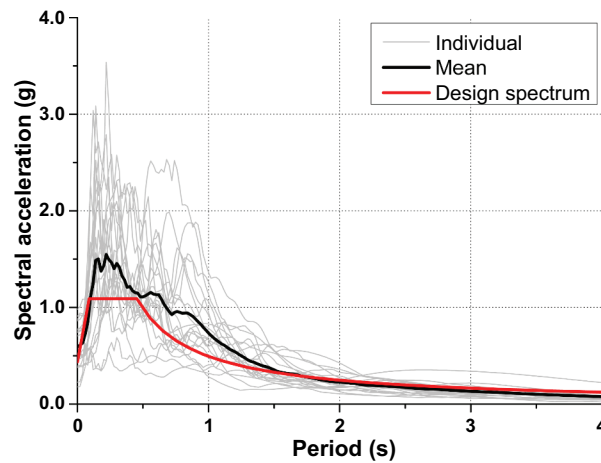


Figure 13. Individual and mean elastic response spectra of DBE ground motions.

SAC project (Gupta and Krawinkler 1998). The DBE records are further scaled up to the maximum considered earthquake (MCE, i.e., probability of exceedance of 2% in 50 years) level by a scale factor of 1.5. The basic information of the ground motions is presented in Table 3.

For the SC-BF, the self-centering devices together with the extended brace parts are placed diagonally in an inverted-V configuration. Simple beam-to-column connections are assumed in order to achieve an economical boundary frame design. Nonlinear response history analysis is conducted, where the building is modelled and analyzed using OpenSees (Mazzoni et al. 2006). A basic 2D centerline model is employed, and the boundary frame members are simulated via nonlinear displacement-based beam-column elements using Steel01 material with a post-yielding stiffness ratio of 0.01. The self-centering braces are simulated with Truss elements, and combined SelfCentering and Elastic-Perfectly Plastic Gap material models are used such that the flag-shaped hysteresis with different behaviours of the loading and unloading plateaus can be captured as shown in Fig. 14. The input parameter values (marked with "\$") of SelfCentering and Elastic-Perfectly Plastic Gap material models are listed in Table 4. The seismic mass assigned to the 2D frame is half of the total structural mass. Leaning columns are built next to the frame so the $P\Delta$ effect is fully considered. Rayleigh damping with a 5% damping ratio for the first and second modes of vibration is adopted.

Modal response spectrum analysis was first conducted to quickly estimate the required base shear and member sizes, where the response modification coefficient (R) and the deflection amplification factor (C_d) were preliminarily taken as 8.0 and 5.0, respectively. Besides, the vertical distribution pattern of seismic force proposed by Chao, Goel, and Lee (2007) is used

Table 3. Basic information of selected ground motions.

SAC Name	Record	Earthquake Magnitude	Distance (km)	PGA (cm/sec ²)	Scale factor	
					DBE	MCE
SE01	Long Beach, Vernon CMD Bldg.	6.5	1.2	348.06	0.64	0.96
SE02	Long Beach, Vernon CMD Bldg.	6.5	1.2	270.82	0.64	0.96
SE03	Morgan Hill, 1984, Gilroy	6.2	15	133.39	3.69	5.54
SE04	Morgan Hill, 1984, Gilroy	6.2	15	228.80	3.69	5.54
SE05	West. Washington, Olympia, 1949	6.5	56	202.25	2.42	3.63
SE06	West. Washington, Olympia, 1949	6.5	56	185.54	2.42	3.63
SE07	West. Washington, Seattle Army B., 1949	6.5	80	54.16	6.94	10.41
SE08	West. Washington, Seattle Army B., 1949	6.5	80	71.40	6.94	10.41
SE09	North Palm Springs, 1986	6	6.7	337.11	2.22	3.33
SE10	North Palm Springs, 1986	6	6.7	326.37	2.22	3.33
SE11	Puget Sound, Wa., Olympia, 1949	7.1	80	171.59	5.59	8.39
SE12	Puget Sound, Wa., Olympia, 1949	7.1	80	135.93	5.59	8.39
SE13	Puget Sound, Wa., Federal OFC B., 1949	7.1	61	68.62	6.86	10.30
SE14	Puget Sound, Wa., Federal OFC B., 1949	7.1	61	56.31	6.86	10.30
SE15	Eastern Wa., Tacoma County, 1949	7.1	60	32.80	11.28	16.93
SE16	Eastern Wa., Tacoma County, 1949	7.1	60	64.92	11.28	16.93
SE17	Llolleo, Chile 1985	8	42	551.83	1.61	2.42
SE18	Llolleo, Chile 1985	8	42	530.56	1.61	2.42
SE19	Vinadel Mar, Chile, 1985	8	42	314.23	2.20	3.30
SE20	Vinadel Mar, Chile, 1985	8	42	223.01	2.20	3.30

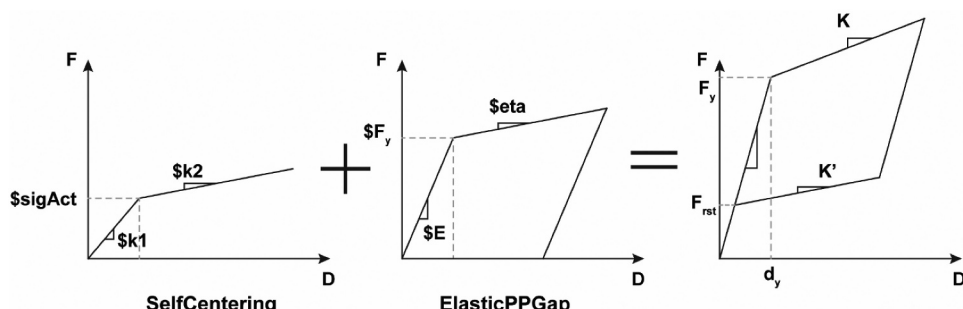


Figure 14. The numerical model of the self-centering braces.

**Table 4.** The modal parameters of self-centering braces and BRBs.

Self-centering braces						
SelfCentering	\$k1 F_{rst}/d_y	\$k2 K'	\$sigAct F_{rst}	\$beta 0		
ElasticPPGap	\$E $(F_y - F_{rst})/d_y$	\$Fy $F_y - F_{rst}$	\$gap 0	\$eta $(K - K')/(F_y - F_{rst})/d_y$		
BRBs						
Steel02	\$Fy 235	\$E0 2.06e5	\$b 0.01	\$R0 20	\$CR1 0.925	\$CR2 0.15
	\$a1 0.03	\$a2 1	\$a3 0.015	\$a4 1		

to allocate greater forces on top of a building (Qiu and Zhu 2017a). Nonlinear response history procedure was subsequently performed to refine the design. The design targets are as follows: 1) the “yield” resistance of the brace is not exceeded under the frequently-occurred earthquake (FOE); and 2) the mean peak inter-story drift does not exceed 2% and 4% under the DBE and MCE, respectively. Based on the above design considerations, the detailed design information of the devices, such as the required size and number of friction springs, is summarised in Table 5. In particular, paralleled friction springs are employed for the devices used on the 1st~4th floors, while only one set of friction springs is used for the devices on the 5th~6th floors due to the relatively small inter-story shear demand. The number of friction springs for the devices is determined such that a stroke of at least 143 mm is provided, corresponding to an inter-story drift of 5%. Recognizing the fact that the actual initial stiffness of the self-centering braces is subjected to uncertainties related to manufacturing, fabrication, and machining tolerance, the initial stiffness of the self-centering braces is provisionally determined to be same as that of the BRBs discussed in the following paragraph. The first mode period of the SC-BF is 0.92s.

The BRBF is designed to have the same base shear as that of the SC-BF, i.e., the BRB and self-centering device at the same floor have the same level of yield resistance. This ensures a direct comparison between the two structural systems, and as a result the mechanism which attributes to the difference in their system-level behaviour can be more clearly revealed. In OpenSees, the BRB elements are modelled using the *Steel02* material which considers isotropic strain hardening (Ariyaratana and Fahnestock 2011; Eatherton, Fahnestock, and Miller 2014).

Table 5. Summary of device design details for prototype buildings.

Story No.	"Yield" strength (kN)	Friction rings						number
		Location	Ring type	H (mm)	D_2 or D_1 (mm)	β	b_2 or b_1 (mm)	
1	1237.3	Outer set	Outer rings	76	370	14.03°	14.5	21
			Inner rings	76	308	14.03°	9	22
		Inner set	Outer rings	60	302	14.03°	12.5	27
			Inner rings	60	250	14.03°	7.5	28
2	1085.6	Outer set	Outer rings	70	330	14.03°	14	22
			Inner rings	70	270	14.03°	9	23
		Inner set	Outer rings	58	264	14.03°	14	26
			Inner rings	58	210	14.03°	7	27
3	999.0	Outer set	Outer rings	66	320	14.03°	14	21
			Inner rings	66	263	14.03°	8	22
		Inner set	Outer rings	54	258	14.03°	14	26
			Inner rings	54	204	14.03°	7.5	27
4	868.4	Outer set	Outer rings	64	310	14.03°	14	22
			Inner rings	64	252	14.03°	8.5	23
		Inner set	Outer rings	50	246	14.03°	13.5	28
			Inner rings	50	195	14.03°	7	29
5	686.0	-	Outer rings	74	350	14.03°	14	20
		-	Inner rings	74	289	14.03°	9	21
6	433.9	-	Outer rings	58	264	14.03°	14	28
		-	Inner rings	58	210	14.03°	7	29

The isotropic hardening parameters of the *Steel02* material, i.e., a1, a2, a3 and a4, as well as other parameters, are calibrated through an experimental hysteretic curve (Black, Makris, and Aiken 2002), as listed in [Table 4](#). The effective length of the BRB is assumed to be 49% of the node-to-node length of the bracing member. As just mentioned, the calculated elastic stiffness values of the BRBs are adopted for the corresponding self-centering braces, and therefore, the first mode period of the BRBF is equal to that of the SC-BF. Finally, a hybrid system (HBF), with one bay adopting self-centering braces and the other bay adopting BRBs, is additionally considered. The HBF exhibits a typical “partial self-centering” response. How does such behavior affect the peak and residual performances of the structure is worth investigation.

4.2. Analysis Results and Discussions

[Figure 15a](#) shows the mean height-wise peak and residual inter-story drifts as well as the peak absolute floor acceleration distributions of the three frames under the DBE. The mean peak inter-story drifts of all the structures do not exceed 2%. Compared with the other two frames, the SC-BF clearly has the largest peak inter-story drift but the smallest (zero) residual inter-story drift. The “high-mode effect” of the SC-BF is pronounced, as indicated by the amplified peak inter-story drift responses at the upper floors. This behavior is caused by reduced energy dissipation, as typically shown in [Fig. 16](#), and the additional high-mode contribution tends to induce a significant concentration of the inter-story drift ratios in the top stories of buildings (Qiu and Zhu 2016). On the other hand, reduced peak inter-story drifts are observed for the BRBF, although the residual inter-story drifts are evidently increased because the permanent deformation is more easily accumulated in the system with a full hysteretic response. The typical force-deformation history of a single BRB is also shown in [Fig. 16](#). A similar trend is observed for the MCE response, as shown in [Fig. 15b](#). The mean peak inter-story drifts are all below 4%, satisfying the ASCE 7-16 requirement. For the three considered structures, no single MCE ground motion leads to the peak inter-story drift exceeding 5%. Note that the BRBF and SC-BF are assumed to have the same base shear/yield resistance for direct

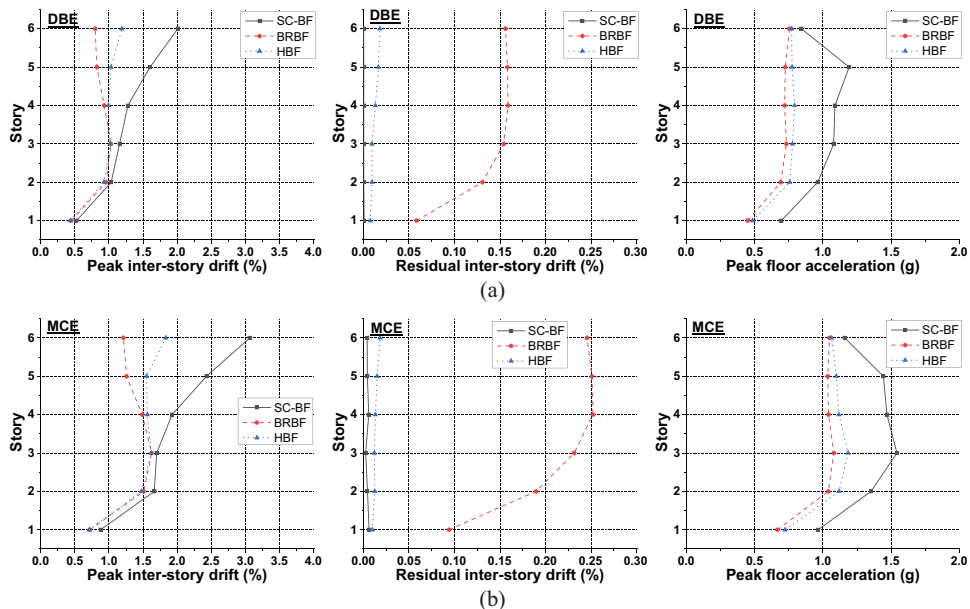


Figure 15. System-level analysis results: a) DBE response, b) MCE response.

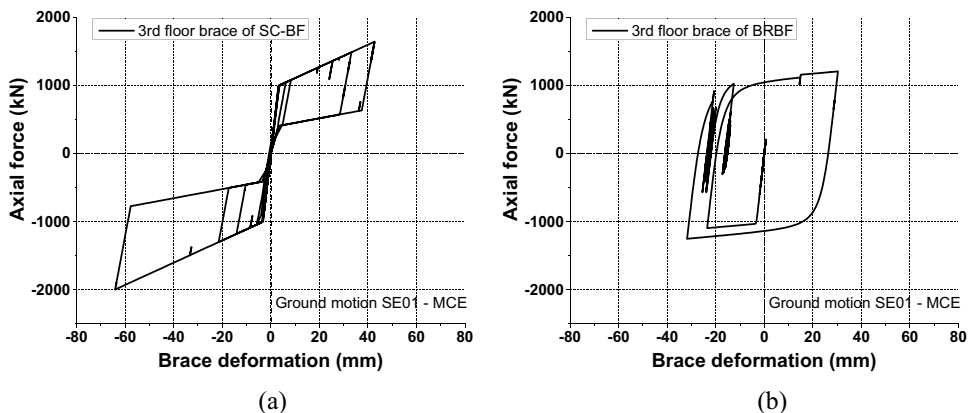


Figure 16. Typical force-deformation response of brace: a) SC-BF, b) BRBF.

comparison, a strategy which may be conservative for the BRBF, resulting in its mean peak inter-story drift ratio being only about 1.5% under the MCE. In other words, the relatively small peak deformation leads to small residual deformation.

Another finding is that the peak floor acceleration response of the SC-BF is larger than the BRBF. Floor acceleration significantly affects the non-structural building performance which is partially responsible for the injuries, fatalities, repair costs and disruption time after an earthquake (Karavasilis and Seo 2011; Shu, Zhang, and Nagarajaiah 2017). Previous studies (Fang et al. 2018; Tremblay, Lacerte, and Christopoulos 2008) suggested that the increased floor acceleration of SC-BFs is caused by the remarkable differences in the shear force between the adjacent stories (i.e., one floor has the shear force lagging that of the neighboring floor during the shaking) as a result of the more abrupt transitions of the flag-shaped hysteresis. It should be noted that in practice the “corners” of the hysteresis of a self-centering device may be less sharp than that assumed in the numerical model, so it is reasonable to deduce that the actual peak floor acceleration may be less pronounced (Wiebe and Christopoulos 2010).

The HBF seems to be quite effective in controlling both the peak and residual deformations. While the peak inter-story drift of the HBF is still larger than that of the BRBF, the value is evidently decreased compared with the SC-BF. Importantly, the residual inter-story drift is remarkably suppressed even though the system itself does not provide a full static self-centering capability. This can be explained by the “probabilistic self-centering” concept, which specifies that the actual residual deformation during an earthquake is often smaller than the maximum possible value obtained by slowly removing the load from the same peak deformation (Eatherton and Hajjar 2011). Therefore, even a partial self-centering behavior can still effectively mitigate the residual deformation during the “dynamic shakedown”. Furthermore, the peak floor acceleration responses of the HBF and BRBF are comparable, both are significantly smaller than that of the SC-BF.

In order to foster a better understanding of the behavior of the structures, Fig. 17 presents some representative individual cases. According to Fig. 17a, the SC-BF exhibits the largest peak inter-story drift as well as the most significant fluctuation. These are attributed to the unique flag-shaped responses of the braces with reduced energy dissipation. Nevertheless, the SC-BF tends to oscillate near the zero deformation line and finally with negligible residual deformation during the attenuation of vibration, whereas the BRBF oscillates with certain excursions of deformation. On the other hand, the HBF can effectively eliminate the residual deformation, and meanwhile the peak deformation is also well controlled. Figure 17b shows the peak floor acceleration time-histories of a typical floor of these structures under the same excitation. Large floor acceleration responses generally occur at the same time, but the amplitudes differ

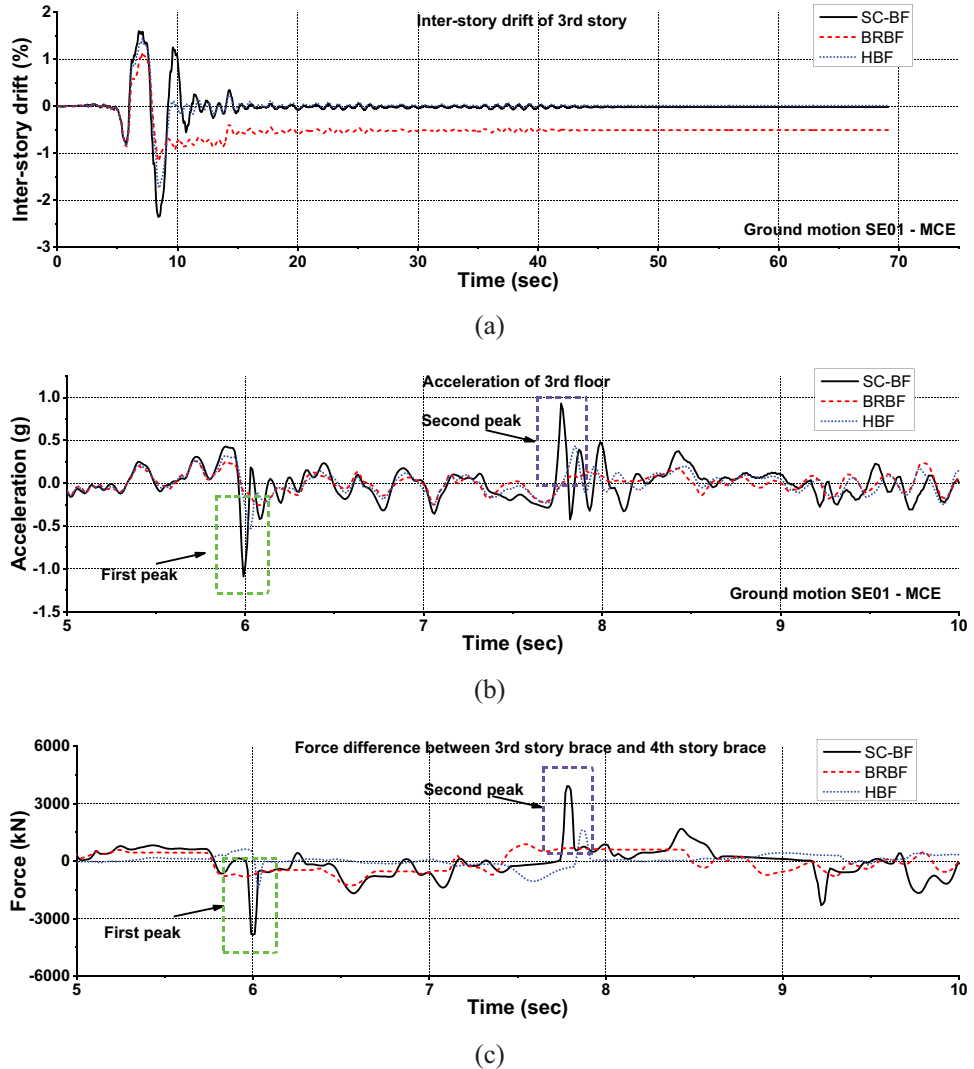


Figure 17. Typical time-history responses: a) inter-story drift, b) floor acceleration, c) inter-story shear force provided by braces.

significantly. Figure 17c confirms that the difference of the inter-story shear force between the adjacent stories is directly responsible for the large peak floor acceleration, where the SC-BF exhibits the most evident inconsistency in the inter-story shear forces. An in-depth investigation of the “high-mode effect” of the SC-BF is also conducted. As shown in Fig. 18, due to the reduced energy dissipation of the SC dampers compared to the BRBs, the dampers at the first story of the SC-BF consume less energy so that more seismic energy is transferred to the top stories. As such, the inter-story drift tends to concentrate in the top stories of the SC-BF. Incidentally, a more suitable design method for SC structures is desirable in the future study.

Judging from the present data, it is believed that the HBF maintains a good balance among the peak/residual drifts and floor acceleration responses. This suggests that the proposed self-centering devices may be more suited to hybrid systems which have multiple energy dissipation sources. In other words, the self-centering devices can be selectively used in critical regions to achieve desirable system-level behavior with a more manageable cost control.

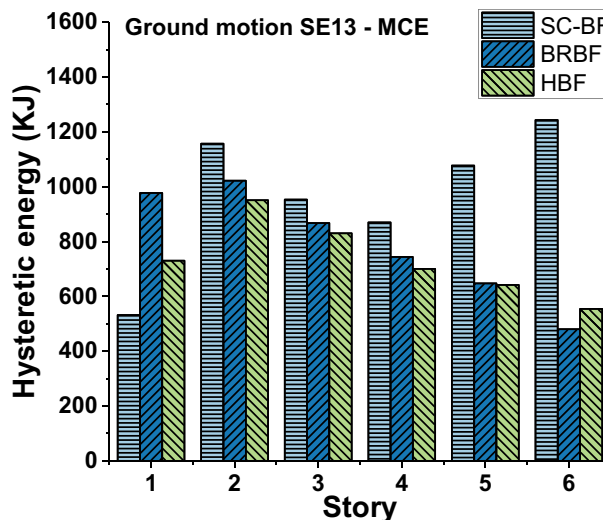


Figure 18. The total hysteretic energy dissipation of braces at different stories.

5. Summary and Conclusions

A new self-centering device equipped with paralleled friction spring groups has been examined in this study. The main advantage of the device is its flexibility in both the load resistance and deformability. The study commenced with a detailed discussion of the fundamental working principle, analytical expression and recommended fabrication procedure of the device. An experimental study was subsequently conducted on three device specimens which varied in taper surface treatment. A system level analysis was finally carried out to evaluate the effectiveness of the devices. The main findings and conclusions are summarized as follows.

- The device specimens showed very stable flag-shaped hysteretic responses with excellent self-centering capability. Negligible degradation was observed during the multiple rounds of cyclic loading, suggesting that the devices are fully reusable after undergoing several major earthquakes. The paralleled friction spring groups were effectively restrained by the guides and hence exhibited anticipated deformation mode.
- The taper surface treatment could affect the hysteretic response of the specimens. Shot blasting was confirmed to be an effective way to increase the friction of the taper surface. In general, an increase in friction leads to larger load resistance and wider hysteresis, but has no critical influence on the initial stiffness of the device.
- Satisfactory energy dissipation was observed with an equivalent viscous damping (EVD) of up to 20%. Large EVDs were induced at small amplitudes, which indicated that the devices could participate in energy dissipation at early stages.
- The behavior of individual friction springs and the global behavior of the device could be well predicted by the analytical model described in this study. However, minor discrepancy is inevitable which may be attributed to the uncertainties related to friction coefficient and machining tolerance.
- The system level analysis showed that the self-centering devices are very effective in eliminating the residual deformation, but tend to increase both the peak deformation and floor acceleration responses. A hybrid system incorporating the self-centering devices together with other energy dissipation providers such as BRBs appears to be a desirable option that simultaneously controls the peak deformation, residual deformation, and peak floor acceleration.

Acknowledgments

The financial supports from the National Natural Science Foundation of China (NSFC) with Grant Nos. 52078366, 51778456, 51820105013 and 51778459 are gratefully acknowledged. Supports for this study were also provided by the State Key Laboratory of Disaster Reduction in Civil Engineering with Grant No. SLDRC19-B-05 and Sustainable Structural Engineering Research Funds from Tongji Architectural Design (Group) Co. Ltd.

Disclosure Statement

No potential conflict of interest was reported by the author(s).

Funding

This work was supported by the National Natural Science Foundation of China (NSFC) with [51778456, 52078366, 51820105013, 51778459].

References

- American Society of Civil Engineers (ASCE). 2016. Minimum design loads for buildings and other structures ASCE 7-16.
- Ariyaratana, C., and L. A. Fahnestock. 2011. Evaluation of buckling-restrained braced frame seismic performance considering reserve strength. *Engineering Structures* 33 (1): 77–89.
- Black, C., N. Makris, and I. Aiken. 2002. Component testing, stability analysis and characterization of buckling restrained braces, PEER report 2002/08, Pacific Earthquake Engineering Research Center. *University of California at Berkeley*.
- Bruneau, M., and G. MacRae. 2017. *Reconstructing Christchurch: A seismic shift in building structural systems.* : Christchurch, New Zealand: The Quake Centre, University of Canterbury.
- Chao, S.-H., S. C. Goel, and S.-S. Lee. 2007. A seismic design lateral force distribution based on inelastic state of structures. *Earthquake Spectra* 23 (3): 547–69. doi: [10.1193/1.2753549](https://doi.org/10.1193/1.2753549).
- Chou, -C.-C., and J.-H. Chen. 2011a. Development of floor slab for steel post-tensioned self-centering moment frames. *Journal of Constructional Steel Research* 67 (10): 1621–35. doi: [10.1016/j.jcsr.2011.04.006](https://doi.org/10.1016/j.jcsr.2011.04.006).
- Chou, -C.-C., T.-H. Wu, A. R. O. Beato, P.-T. Chung, and Y.-C. Chen. 2016. Seismic design and tests of a full-scale one-story one-bay steel frame with a dual-core self-centering brace. *Engineering Structures* 111: 435–50. doi: [10.1016/j.engstruct.2015.12.007](https://doi.org/10.1016/j.engstruct.2015.12.007).
- Chou, -C.-C., Y.-C. Chen, D.-H. Pham, and V.-M. Truong. 2014. Steel braced frames with dual-core SCBs and sandwiched BRBs: mechanics, modeling and seismic demands. *Engineering Structures* 72: 26–40. doi: [10.1016/j.engstruct.2014.04.022](https://doi.org/10.1016/j.engstruct.2014.04.022).
- Chou, C. C., and J. H. Chen. 2011b. Seismic design and shake table tests of a steel post-tensioned self-centering moment frame with a slab accommodating frame expansion. *Earthquake Engineering & Structural Dynamics* 40 (11): 1241–61. doi: [10.1002/eqe.1086](https://doi.org/10.1002/eqe.1086).
- Christopoulos, C., R. Tremblay, H. J. Kim, and M. Lacerte. 2008. Self-centering energy dissipative bracing system for the seismic resistance of structures: development and validation. *Journal of Structural Engineering-Asce* 134 (1): 96–107. doi: [10.1061/\(ASCE\)0733-9445\(2008\)134:1\(96\)](https://doi.org/10.1061/(ASCE)0733-9445(2008)134:1(96)).
- Clark, P., K. Frank, H. Krawinkler, and R. Shaw. 1997. Protocol for fabrication, inspection, testing, and documentation of beam-column connection tests and other experimental specimens. SAC Steel Project Background Document (Report No. SAC/BD-97/02).
- Dong, H., X. Du, Q. Han, H. Hao, K. Bi, and X. Wang. 2017. Performance of an innovative self-centering buckling restrained brace for mitigating seismic responses of bridge structures with double-column piers. *Engineering Structures* 148: 47–62. doi: [10.1016/j.engstruct.2017.06.011](https://doi.org/10.1016/j.engstruct.2017.06.011).
- Eatherton, M. R., and J. F. Hajjar. 2011. Residual drifts of self-centering systems including effects of ambient building resistance *Earthquake Spectra* 27 (3): 719–44.
- Eatherton, M. R., L. A. Fahnestock, and D. J. Miller. 2014. Computational study of self-centering buckling-restrained braced frame seismic performance. *Earthquake Engineering & Structural Dynamics* 43 (13): 1897–914. doi: [10.1002/eqe.2428](https://doi.org/10.1002/eqe.2428).
- Erochko, J., C. Christopoulos, and R. Tremblay. 2015a. Design, testing, and detailed component modeling of a high-capacity self-centering energy-dissipative brace. *Journal of Structural Engineering* 141 (8): 04014193. doi: [10.1061/\(ASCE\)ST.1943-541X.0001166](https://doi.org/10.1061/(ASCE)ST.1943-541X.0001166).



- Erochko, J., C. Christopoulos, and R. Tremblay. 2015b. Design and testing of an enhanced-elongation telescoping self-centering energy-dissipative brace. *Journal of Structural Engineering* 141 (6): 04014163. doi: [10.1061/\(ASCE\)ST.1943-541X.0001109](https://doi.org/10.1061/(ASCE)ST.1943-541X.0001109).
- Erochko, J., C. Christopoulos, R. Tremblay, and H. J. Kim. 2013. Shake table testing and numerical simulation of a self-centering energy dissipative braced frame. *Earthquake Engineering & Structural Dynamics* 42 (11): 1617–35. doi: [10.1002/eqe.2290](https://doi.org/10.1002/eqe.2290).
- Fang, C., M. C. H. Yam, A. C. C. Lam, and Y. Zhang. 2015a. Feasibility study of shape memory alloy ring spring systems for self-centring seismic resisting devices. *Smart Materials and Structures* 24 (7): 075024. doi: [10.1088/0964-1726/24/7/075024](https://doi.org/10.1088/0964-1726/24/7/075024).
- Fang, C., M. C. H. Yam, H. Ma, and K. F. Chung. 2015b. Tests on superelastic Ni-Ti SMA bars under cyclic tension and direct-shear: Towards practical recentring connections. *Materials and Structures* 48 (4): 1013–30. doi: [10.1617/s11527-013-0212-4](https://doi.org/10.1617/s11527-013-0212-4).
- Fang, C., M. C. Yam, A. C. Lam, and L. Xie. 2014. Cyclic performance of extended end-plate connections equipped with shape memory alloy bolts. *Journal of Constructional Steel Research* 94: 122–36.
- Fang, C., Q. Zhong, W. Wang, S. Hu, and C. Qiu. 2018. Peak and residual responses of steel moment-resisting and braced frames under pulse-like near-fault earthquakes. *Engineering Structures* 177: 579–97. doi: [10.1016/j.engstruct.2018.10.013](https://doi.org/10.1016/j.engstruct.2018.10.013).
- Fang, C., W. Wang, C. He, and Y. Chen. 2017. Self-centring behaviour of steel and steel-concrete composite connections equipped with NiTi SMA bolts. *Engineering Structures* 150: 390–408. doi: [10.1016/j.engstruct.2017.07.067](https://doi.org/10.1016/j.engstruct.2017.07.067).
- Fang, C., W. Wang, and D. Shen. 2021. Development and experimental study of disc spring-based self-centering devices for seismic resilience. *Journal of Structural Engineering* 147 (7): 04021094. doi: [10.1061/\(ASCE\)ST.1943-541X.0003058](https://doi.org/10.1061/(ASCE)ST.1943-541X.0003058).
- Fang, C., W. Wang, and W. Feng. 2019. Experimental and numerical studies on self-centring beam-to-column connections free from frame expansion. *Engineering Structures* 198: 109526.
- Fang, C., X. Zhou, A. I. Osofero, Z. Shu, and M. Corradi. 2016. Superelastic SMA Belleville washers for seismic resisting applications: Experimental study and modelling strategy. *Smart Materials and Structures* 25 (10): 105013. doi: [10.1088/0964-1726/25/10/105013](https://doi.org/10.1088/0964-1726/25/10/105013).
- Fang, C., Y. Ping, Y. Zheng, and Y. Chen. 2021. Probabilistic economic seismic loss estimation of steel braced frames incorporating emerging self-centering technologies. *Engineering Structures* 241: 112486. doi: [10.1016/j.engstruct.2021.112486](https://doi.org/10.1016/j.engstruct.2021.112486).
- Feng, W., C. Fang, and W. Wang. 2019. Behavior and design of top flange-rotated self-centering steel connections equipped with SMA ring spring dampers. *Journal of Constructional Steel Research* 159: 315–29. doi: [10.1016/j.jcsr.2019.04.046](https://doi.org/10.1016/j.jcsr.2019.04.046).
- Filiatrault, A., R. Tremblay, and R. Kar. 2000. Performance evaluation of friction spring seismic damper. *Journal of Structural Engineering* 126 (4): 491–99. doi: [10.1061/\(ASCE\)0733-9445\(2000\)126:4\(491\)](https://doi.org/10.1061/(ASCE)0733-9445(2000)126:4(491)).
- Garlock, M. E., and J. Li. 2008. Steel self-centering moment frames with collector beam floor diaphragms. *Journal of Constructional Steel Research* 64 (5): 526–38. doi: [10.1016/j.jcsr.2007.10.006](https://doi.org/10.1016/j.jcsr.2007.10.006).
- Gupta, A., and H. Krawinkler. 1998. Seismic demands for the performance evaluation of steel moment resisting frame structures. (SAC Task 5.4.3). Report No. 132, John A. Blume Earthquake Engineering Center, Stanford University, CA.
- Hill, K. 1995. The utility of ring springs in seismic isolation systems. PhD Thesis, University of Canterbury.
- Huang, X., M. R. Eatherton, and Z. Zhou. 2020. Initial stiffness of self-centering systems and application to self-centering-beam moment-frames. *Engineering Structures* 203: 109890.
- Jiang, Z.-Q., C. Dou, A.-L. Zhang, Q. Wang, and Y.-X. Wu. 2019a. Experimental study on earthquake-resilient prefabricated cross joints with L-shaped plates. *Engineering Structures* 184: 74–84. doi: [10.1016/j.engstruct.2019.01.067](https://doi.org/10.1016/j.engstruct.2019.01.067).
- Jiang, Z.-Q., X.-F. Yang, C. Dou, C. Li, and A.-L. Zhang. 2019b. Cyclic testing of replaceable damper: Earthquake-resilient prefabricated column-flange beam-column joint. *Engineering Structures* 183: 922–36. doi: [10.1016/j.engstruct.2019.01.060](https://doi.org/10.1016/j.engstruct.2019.01.060).
- Karavasilis, T. L., and C.-Y. Seo. 2011. Seismic structural and non-structural performance evaluation of highly damped self-centering and conventional systems. *Engineering Structures* 33 (8): 2248–58. doi: [10.1016/j.engstruct.2011.04.001](https://doi.org/10.1016/j.engstruct.2011.04.001).
- Khoo, -H.-H., C. Clifton, J. Butterworth, and G. MacRae. 2013. Experimental study of full-scale self-centering sliding hinge joint connections with friction ring springs. *Journal of Earthquake Engineering* 17 (7): 972–97. doi: [10.1080/13632469.2013.787378](https://doi.org/10.1080/13632469.2013.787378).
- Khoo, H. H., C. Clifton, J. Butterworth, G. Macrae, S. Gledhill, and G. Sidwell. 2012. Development of the self-centering sliding hinge joint with friction ring springs. *Journal of Constructional Steel Research* 78 (6): 201–11. doi: [10.1016/j.jcsr.2012.07.006](https://doi.org/10.1016/j.jcsr.2012.07.006).
- Li, Z., M. He, and K. Wang. 2018. Hysteretic performance of self-centering glulam beam-to-column connections. *Journal of Structural Engineering* 144 (5): 04018031. doi: [10.1061/\(ASCE\)ST.1943-541X.0002012](https://doi.org/10.1061/(ASCE)ST.1943-541X.0002012).

- Lin, Y.-C., R. Sause, and J. M. Ricles. 2013. Seismic performance of steel self-centering, moment-resisting frame: Hybrid simulations under design basis earthquake. *Journal of Structural Engineering* 139 (11): 1823–32. doi: [10.1061/\(ASCE\)ST.1943-541X.0000745](https://doi.org/10.1061/(ASCE)ST.1943-541X.0000745).
- Mazzoni, S., F. McKenna, M. H. Scott, and G. L. Fenves. 2006. OpenSees command language manual. Pacific Earthquake Engineering Research (PEER) Center, 264.
- McCormick, J., H. Aburano, M. Ikenaga, and M. Nakashima. 2008. Permissible residual deformation levels for building structures considering both safety and human elements. *Proceedings of the 14th world conference on earthquake engineering*, Beijing, China.
- Miller, D. J., L. A. Fahnestock, and M. R. Eatherton. 2012. Development and experimental validation of a nickel-titanium shape memory alloy self-centering buckling-restrained brace. *Engineering Structures* 40: 288–98.
- National Research Council. 2011. *National earthquake resilience: Research, implementation, and outreach*. Washington, D.C.: National Academies Press.
- Ping, Y., C. Fang, Y. Chen, and M. C. H. Yam. 2021. Seismic robustness of self-centering braced frames suffering tendon failure. *Earthquake Engineering & Structural Dynamics* 50 (6): 1671–91. doi: [10.1002/eqe.3421](https://doi.org/10.1002/eqe.3421).
- Qiu, C.-X., and S. Zhu. 2016. High-mode effects on seismic performance of multi-story self-centering braced steel frames. *Journal of Constructional Steel Research* 119: 133–43. doi: [10.1016/j.jcsr.2015.12.008](https://doi.org/10.1016/j.jcsr.2015.12.008).
- Qiu, C., H. Li, K. Ji, H. Hou, and L. Tian. 2017. Performance-based plastic design approach for multi-story self-centering concentrically braced frames using SMA braces. *Engineering Structures* 153: 628–38. doi: [10.1016/j.engstruct.2017.10.068](https://doi.org/10.1016/j.engstruct.2017.10.068).
- Qiu, C., and S. Zhu. 2017a. Performance-based seismic design of self-centering steel frames with SMA-based braces. *Engineering Structures* 130: 67–82. doi: [10.1016/j.engstruct.2016.09.051](https://doi.org/10.1016/j.engstruct.2016.09.051).
- Qiu, C., and S. Zhu. 2017b. Shake table test and numerical study of self-centering steel frame with SMA braces. *Earthquake Engineering & Structural Dynamics* 46 (1): 117–37. doi: [10.1002/eqe.2777](https://doi.org/10.1002/eqe.2777).
- Ricles, J. M., R. Sause, M. M. Garlock, and C. Zhao. 2001. Posttensioned seismic-resistant connections for steel frames. *Journal of Structural Engineering* 127 (2): 113–21. doi: [10.1061/\(ASCE\)0733-9445\(2001\)127:2\(113\)](https://doi.org/10.1061/(ASCE)0733-9445(2001)127:2(113)).
- Ricles, J. M., R. Sause, S. Peng, and L. Lu. 2002. Experimental evaluation of earthquake resistant posttensioned steel connections. *Journal of Structural Engineering* 128 (7): 850–59. doi: [10.1061/\(ASCE\)0733-9445\(2002\)128:7\(850\)](https://doi.org/10.1061/(ASCE)0733-9445(2002)128:7(850)).
- Riley, M., C. Stark, L. Kempner Jr., and W. Mueller. 2006. Seismic retrofit using spring damper devices on high-voltage equipment stands. *Earthquake Spectra* 22 (3): 733–53. doi: [10.1193/1.2216736](https://doi.org/10.1193/1.2216736).
- Shu, Z., J. Zhang, and S. Nagarajaiah. 2017. Dimensional analysis of inelastic structures with negative stiffness and supplemental damping devices. *Journal of Structural Engineering* 143 (3): 04016184. doi: [10.1061/\(ASCE\)ST.1943-541X.0001658](https://doi.org/10.1061/(ASCE)ST.1943-541X.0001658).
- Tremblay, R., M. Lacerte, and C. Christopoulos. 2008. Seismic response of multistory buildings with self-centering energy dissipative steel braces. *Journal of Structural Engineering* 134 (1): 108–20. doi: [10.1061/\(ASCE\)0733-9445\(2008\)134:1\(108\)](https://doi.org/10.1061/(ASCE)0733-9445(2008)134:1(108)).
- Wang, B., S. Zhu, C.-X. Qiu, and H. Jin. 2019a. High-performance self-centering steel columns with shape memory alloy bolts: design procedure and experimental evaluation. *Engineering Structures* 182: 446–58. doi: [10.1016/j.engstruct.2018.12.077](https://doi.org/10.1016/j.engstruct.2018.12.077).
- Wang, W., C. Fang, D. Shen, R. Zhang, J. Ding, and W. Honglei. 2021. Performance assessment of disc spring-based self-centering braces for seismic hazard mitigation. *Engineering Structures* 242: 112527. doi: [10.1016/j.engstruct.2021.112527](https://doi.org/10.1016/j.engstruct.2021.112527).
- Wang, W., C. Fang, and J. Liu. 2016. Large size superelastic SMA bars: Heat treatment strategy, mechanical property and seismic application. *Smart Materials and Structures* 25 (7). doi: [10.1088/0964-1726/25/7/075014](https://doi.org/10.1088/0964-1726/25/7/075014).
- Wang, W., C. Fang, and J. Liu. 2017. Self-centering beam-to-column connections with combined superelastic SMA bolts and steel angles. *Journal of Structural Engineering* 143 (2): 04016175. doi: [10.1061/\(ASCE\)ST.1943-541X.0001675](https://doi.org/10.1061/(ASCE)ST.1943-541X.0001675).
- Wang, W., C. Fang, X. Yang, Y. Chen, J. Ricles, and R. Sause. 2017. Innovative use of a shape memory alloy ring spring system for self-centering connections. *Engineering Structures* 153: 503–15. doi: [10.1016/j.engstruct.2017.10.039](https://doi.org/10.1016/j.engstruct.2017.10.039).
- Wang, W., C. Fang, Y. Zhao, R. Sause, S. Hu, and J. Ricles. 2019b. Self-centering friction spring dampers for seismic resilience. *Earthquake Engineering & Structural Dynamics* 48 (9): 1045–65. doi: [10.1002/eqe.3174](https://doi.org/10.1002/eqe.3174).
- Wiebe, L., and C. Christopoulos. 2010. Characterizing acceleration spikes due to stiffness changes in nonlinear systems. *Earthquake Engineering & Structural Dynamics* 39 (14): 1653–70. doi: [10.1002/eqe.1009](https://doi.org/10.1002/eqe.1009).
- Wood, A., I. Noy, and M. Parker. 2016. The Canterbury rebuild five years on from the Christchurch earthquake. *The Reserve Bank of New Zealand Bulletin* 79 (3): 3.
- Xie, Q., Z. Zhou, J. H. Huang, D. P. Zhu, and S. P. Meng. 2017. Finite-element analysis of dual-tube self-centering buckling-restrained braces with composite tendons. *Journal of Composites for Construction* 21 (3): 3. doi: [10.1061/\(ASCE\)CC.1943-5614.0000778](https://doi.org/10.1061/(ASCE)CC.1943-5614.0000778).
- Xu, L.-H., X.-W. Fan, and Z.-X. Li. 2016. Development and experimental verification of a pre-pressed spring self-centering energy dissipation brace. *Engineering Structures* 127: 49–61. doi: [10.1016/j.engstruct.2016.08.043](https://doi.org/10.1016/j.engstruct.2016.08.043).
- Xu, L., X. Fan, and Z. Li. 2017a. Cyclic behavior and failure mechanism of self-centering energy dissipation braces with pre-pressed combination disc springs. *Earthquake Engineering & Structural Dynamics* 46 (7): 1065–80. doi: [10.1002/eqe.2844](https://doi.org/10.1002/eqe.2844).

- Xu, L., X. Fan, and Z. Li. 2017b. Experimental behavior and analysis of self-centering steel brace with pre-pressed disc springs. *Journal of Constructional Steel Research* 139: 363–73. doi: [10.1016/j.jcsr.2017.09.021](https://doi.org/10.1016/j.jcsr.2017.09.021).
- Xu, X., Y. Zhang, and Y. Luo. 2016. Self-centering eccentrically braced frames using shape memory alloy bolts and post-tensioned tendons. *Journal of Constructional Steel Research* 125: 190–204. doi: [10.1016/j.jcsr.2016.06.017](https://doi.org/10.1016/j.jcsr.2016.06.017).
- Yam, M. C. H., C. Fang, A. C. C. Lam, and Y. Zhang. 2015. Numerical study and practical design of beam-to-column connections with shape memory alloys. *Journal of Constructional Steel Research* 104: 177–92. doi: [10.1016/j.jcsr.2014.10.017](https://doi.org/10.1016/j.jcsr.2014.10.017).
- Zhang, A.-L., Y.-X. Zhang, R. Li, and Z.-Y. Wang. 2016. Cyclic behavior of a prefabricated self-centering beam–column connection with a bolted web friction device. *Engineering Structures* 111: 185–98. doi: [10.1016/j.engstruct.2015.12.025](https://doi.org/10.1016/j.engstruct.2015.12.025).
- Zhou, Z., Q. Xie, X. C. Lei, X. T. He, and S. P. Meng. 2015. Experimental investigation of the hysteretic performance of dual-tube self-centering buckling-restrained braces with composite tendons. *Journal of Composites for Construction* 19 (6): 6. doi: [10.1061/\(ASCE\)CC.1943-5614.0000565](https://doi.org/10.1061/(ASCE)CC.1943-5614.0000565).